

Solving multiscale dynamical systems by deep learning

Zhi-Qin John Xu^{a,c,1,2}, Junjie Yao^{a,1}, Yuxiao Yi^{a,1}, Liangkai Hang^a, Weinan E^{c,d}, Yaoyu Zhang^{a,b,2}, and Tianhan Zhang^{e,c,d,2}

^aInstitute of Natural Sciences, School of Mathematical Sciences, MOE-LSC and Qing Yuan Research Institute, Shanghai Jiao Tong University; ^bShanghai Center for Brain Science and Brain-Inspired Technology; ^cCenter for Machine Learning Research, School of Mathematical Sciences, Peking University; ^dAI for Science Institute, Beijing; ^eDepartment of Mechanics and Aerospace Engineering, Southern University of Science and Technology

¹Z.X. and J.Y., and Y.Y. contributed equally to this work.

²To whom correspondence should be addressed. E-mail: xuzhiqin@sjtu.edu.cn or zhyy.sjtu@sjtu.edu.cn or zhangth@sustech.edu.cn

Multiscale dynamical systems, modeled by high-dimensional stiff ordinary differential equations (ODEs) with wide-ranging characteristic timescales, arise across diverse fields of science and engineering, but their numerical solvers often encounter severe efficiency bottlenecks. This paper introduces a novel DeePODE method, which consists of a global multiscale sampling method and a fitting by deep neural networks to handle multiscale systems. DeePODE's primary contribution is to address the multiscale challenge of efficiently uncovering representative training sets by combining the Monte Carlo method and the ODE system's intrinsic evolution without suffering from the "curse of dimensionality". The DeePODE method is validated in multiscale systems from diverse areas, including a predator-prey model, a power system oscillation, a battery electrolyte auto-ignition, and turbulent flames. Our methods exhibit strong generalization capabilities to unseen conditions, highlighting the power of deep learning in modeling intricate multiscale dynamical processes across science and engineering domains.

deep learning | ordinary differential equations | multiscale | high dimension

Introduction

Multiscale dynamical systems frequently arise in various scientific problems, including chemical kinetics [1], generic circuit simulation [2], ecosystem evolution [3], oscillation in power systems [4], and biological neural network modeling [5]. Such a multiscale dynamical system often exhibits widespread characteristic timescales and can be modeled by high-dimensional stiff ordinary differential equations (ODEs). Classical numerical solvers require a small timestep to guarantee numerical stability, resulting in high computational costs. Consequently, over the decades, a sustained effort has been made to develop efficient and robust numerical methods to simulate multiscale systems across diverse scientific disciplines.

Machine learning approaches have been introduced to solve high-dimensional multiscale ODEs, but the neural network structure or limited training data often constrains their generality. For example, physics-informed neural networks [6, 7] require a large training cost but only apply for a specific initial condition, preventing their applications in complex spatiotemporal systems such as turbulent flames [8] and biological neural networks [9]. Another frequently employed machine learning methodology focuses on the state mapping function, whose input is the current state and output is the subsequent state or the state change after a specific small or even large time step size. This approach can enhance generality once sufficient training data covers the dynamical evolution trajectories in phase space.

How to obtain sufficient data to represent a multiscale dynamical system in the interested high-dimensional space is critical for deep neural network (DNN) training and generalization in application. The Monte Carlo (MC) method breaks "curse of dimensionality", but with extremely low efficiency, i.e., the error decreases with sample number M by rate $1/\sqrt{M}$. As an example for illustration, the concentration of measure shows that uniformly random samples concentrate on the surface of the high-dimensional sphere [10]. Tabulation approach [11, 12] or manifold sampling (sampling from a set of evolution trajectories) in flame simulation [13, 14, 15, 16, 17, 18, 19, 20, 21, 22] mainly tackle such problem by dimension reduction, which can only work for low-dimensional systems or few working conditions. Suc-

cessful examples often utilize the intrinsic characteristics of considered problems. For example, the key in AlphaGo for solving the Go problem is the high-efficiency sampling in high-dimensional space by MC tree search [23]; Invertible DNNs are used to transform the complex distribution of equilibrium states of protein folding that is difficult for sampling to one that is much simpler for sampling [24].

Compared with the intractable complexity of many problems, such as the Bellman equation in AlphaGo [23], multiscale problems with explicit ODE models have a distinct advantage in that the governing equations can provide substantial information about the target function across the high-dimensional space. In this work, we propose a DeePODE method, which consists of two parts, i.e., firstly, a global multiscale sampling method that incorporates the characteristics of evolutionary dynamical systems and the Monte Carlo method; secondly, a deep neural network for fitting the data. DeePODE provides efficient DNN surrogate models for high-dimensional multiscale dynamical systems.

The DeePODE method utilizes the MC method to sample globally, thereby overcoming the curse of dimensionality. Subsequently, each sample is evolved briefly using the governing ODEs, which imparts multiscale information from the system to the sample set. This means that low change rate regions receive more samples compared with the MC method. The DeePODE method is adaptive to the local characteristics of the target function via the given governing equations. Therefore, DeePODE can effectively approximate the data distribution over various working conditions with reasonable data size.

We demonstrate the effectiveness of DeePODE in various multiscale systems, including a predator-prey model, an electronic dynamical process, a battery electrolyte auto-ignition, and combustion. These systems are important in many applications. For example, computing chemical reaction rates in direct numerical simulation (DNS) [25], Reynolds averaged Navier Stokes (RANS), or large eddy simulation (LES) is a typical difficult problem of combustion in simulating launching rockets, flying planes, and powering automobiles etc [26, 27, 28]. The difficulty originates from multiple aspects, for example, the high dimension of a combustion process involving many species, time scales across eight orders of magnitudes, and highly

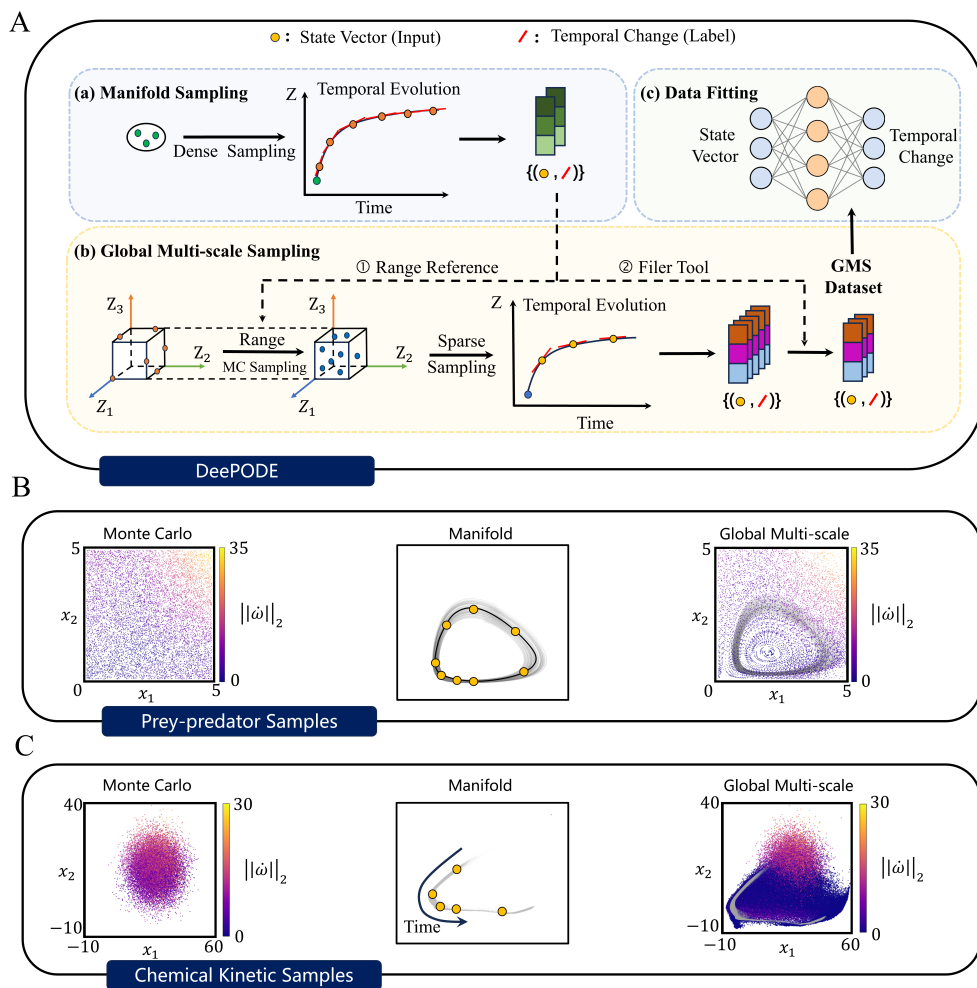


Fig. 1. Schematic diagram of the DeePODE method. (A) Flowchart of DeePODE method. After obtaining a manifold dataset and an MC dataset, each point of the MC dataset is taken as the initial condition of a corresponding dynamical system. Sample along the evolution trajectory of MC data sparsely and filter them by the temporal gradient range of the manifold dataset. The remaining data composes the final GMS dataset. A DNN is used to fit the dataset. (B) Example of prey-predator system. The left and right figures represent the data distribution obtained by the Monte-Carlo and the GMS methods, respectively, and the color of the data points represents the change's norm. The gray regions in the second and third figures represent some evolution trajectories of this system. The yellow points mean the sampled point in the GMS method. (C) Example of Chemical kinetic system. Three figures serve the same purpose as the corresponding figures in (B) except that x_1 and x_2 are the data projected onto the first two principal directions of the manifold dataset.

turbulent dynamics. Our method can handle large mechanisms with many species (more than 50), and one DNN model can accurately predict its chemical kinetics in various unseen cases with different working conditions, even in turbulent flames. The DeePODE models can easily couple with different computational fluid dynamics (CFD) codes and is much faster (two orders of magnitude) than traditional solvers. As combustion is a typical ODE example, it is reasonable to expect that the DeePODE method could be easily extended to more applications, such as biomass chemical kinetics [29] and air pollution problems [30].

Methodology

In this section, we introduce DeePODE by demonstrating its two parts, that is, global multiscale sampling (GMS) and deep neural network (DNN) fitting.

Training data by GMS method. GMS (global multiscale sampling) comprises three steps, i.e., manifold sampling, Monte-Carlo sampling,

and multiscale sampling. The manifold sampling is to evolve the given ODEs with a set of initial conditions, and then data are sampled from the evolving trajectories. Based on the manifold sampling, we can determine the range of each variable. Next, the MC sampling will randomly sample each variable from its corresponding range. Finally, in the multiscale sampling stage, each MC sample will evolve a short trajectory following the ODEs, and data will be sampled from the trajectory, that is, sampling from the manifold around each sample. Therefore, GMS can also be interpreted as global manifold sampling. The Appendix provides a detailed elaboration of GMS for a general ODE system. In the following, we use chemical kinetics as an example to describe GMS. A sampling sketch is illustrated in Fig. 1.

Manifold (MF) sampling. Given different initial temperatures, pressures, and equivalence ratios (reflecting the ratio of air and fuel), the trajectories of all species form a low-dimensional manifold [31]. Manifold sampling comprises two parts. First, we sample from zero-dimensional auto-ignitions, where heated, homogeneous fuel and oxy-

gen ignite spontaneously. The initial temperature (T) range is set so that the ignition delay time belongs to $[0.1\text{ms}, 10\text{ms}]$. Initial pressure P belongs to $[0.5\text{atm}, 2\text{atm}]$. Equivalence ratio ϕ belongs to $[0.5, 3]$. We use the open-source chemical kinetics library Cantera* to run ~ 5000 cases with random initial conditions and maximal time step size 10^{-8}s until maximal running time (e.g., 10ms) or when the temperature change is smaller than 0.001 within 10^{-7}s . We sample each state $\mathbf{x}(t) = [T(t), P(t), Y_1(t), \dots, Y_{n_s}(t)]$ (Y_i is the mass fraction of species i) on each trajectory every 10^{-7}s and its corresponding label $\mathbf{u}(t) = \mathbf{x}(t + \Delta t) - \mathbf{x}(t)$, where $\Delta t = 10^{-6}\text{s}$ is the step size we use for DNN model. The other is sampling from one-dimensional freely propagating premixed flame example at 1 atm, $\phi = 1$, and temperature is set from 300K to 1000K (every 10K). The physical length is 0.03m with 800 grid points. We sample from the stable states of grids. Both zero-dimensional and one-dimensional data constitute the manifold sample set, which is denoted as $D_{\text{man}} = \{(\mathbf{x}(t), \mathbf{u}(t))\}$.

Monte-Carlo (MC) sampling. Next, we perform a global Monte-Carlo sampling. The pressure range is the same as for manifold sampling. The ranges of temperature and mass fractions of species are determined by the corresponding range in D_{man} . Each data point $\mathbf{x}(t)$ is sampled uniformly in the log scale within the given range by the Monte-Carlo method with a sample size of approximately 3,200,000. The label for $\mathbf{x}(t)$ is computed by Cantera as $\mathbf{u}(t) = \mathbf{x}(t + \Delta t) - \mathbf{x}(t)$. Each data point is filtered by the manifold data as follows. A data point is kept if each element of its label belongs to a range determined by the manifold data, i.e., $\mathbf{u}(t)_i \in [\lambda_1 \mathbf{u}_{\text{min},i}, \lambda_2 \mathbf{u}_{\text{max},i}]$, where $\mathbf{u}_{\text{min},i}$ (can be negative) and $\mathbf{u}_{\text{max},i}$ are the minimum and maximum of the i -th element in the labels of all manifold data, respectively, λ_1 and λ_2 are hyper-parameters.

Multiscale (MS) sampling. For each input of the filtered data, we simulate a short reaction trajectory and sample several data points from the trajectory. Thus, the new dataset has multiscale information embedded in the ODE system. The new dataset is filtered again by the manifold data D_{man} to obtain the final training dataset.

Deep neural network. The input is the Box-Cox transformation (BCT) [32] of a state vector $\mathbf{x}(t)$, and the output is to fit the BCT of $\mathbf{u}(t) = \mathbf{x}(t + \Delta t) - \mathbf{x}(t)$, where $\Delta t = 10^{-6}\text{s}$. Note that the BCT of x is $(x^\lambda - 1)/\lambda$ with λ is set as 0.1. As indicated by the frequency principle [33, 34], the neural network is difficult to learn small-scale components, and BCT is an effective way to alleviate such difficulty [8].

The structure is as follows. In the first hidden layer, the input \mathbf{x} undergoes an affine transformation with trainable weights $\mathbf{W}^{[1]}$ and biases $\mathbf{b}^{[1]}$, followed by a GELU activation function, i.e., $\sigma(\mathbf{W}^{[1]}\mathbf{x} + \mathbf{b}^{[1]})$. Iteratively, the output of the previous hidden layer is used as the input of the subsequent hidden layer until the output layer. The hidden layer widths in this work are usually 3200-1600-800-400 for combustion. The loss function is the mean absolute error. The training algorithm is Adam with batch size 1024 and learning rate 10^{-4} .

Results and discussion

Two-dimensional multiscale predator-prey model. For illustration, we first apply the DeePODE method for a two-dimensional multiscale predator-prey model [35]. We use this simple example to illustrate that DeePODE can have the advantage of both Monte-Carlo sampling and manifold sampling. Consider a two-dimensional Lotka-Volterra Predator-Prey Model: $dx_1/dt = -x_1 + x_1x_2$ and

$dx_2/dt = 2x_2 - x_1x_2$. The DNN used in this example consists of three hidden layers with sizes 200, 200, and 200, respectively, mapping the current state to the state after $\delta t = 0.1$.

We first use the Monte-Carlo method to randomly sample 100,000 data points within the range of $x_1 \in [0, 5]$ and $x_2 \in [0, 5]$ as initial values for the dynamical system. Due to stiffness constraints, the corresponding labels are obtained through direct integration with an integration time step size not exceeding 10^{-2} . For DeePODE, we randomly sample 20,000 data points within the aforementioned range, and then evolve them with time step size not exceeding 10^{-2} . Then, we further sample states at evolution time 0.1s, 0.2s, 0.3s and 0.4s, resulting in a total of 100,000 samples. Similarly, manifold sampling involves evolving a small number of initial values for a long period of time. In our example, manifold sampling randomly selects 500 initial samples, and for each initial value, 200 points are picked along its integral curve with a fixed step size of 0.1s. This results in a total of 100,000 samples obtained from 500 trajectories.

As shown in Fig. 1(B), the MC method treats all space equally, while DeePODE has more samples in the low change rate region. The data distribution of the manifold method is in Appendix Fig. S1. As shown in Fig. 2, the DNNs trained by the MC method and manifold method deviate from the reference solution while the one by the DeePODE method can well predict the reference solution even $t = 50\text{s}$.

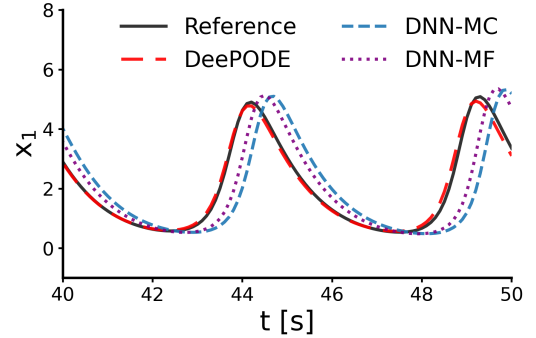


Fig. 2. Two-dimensional predator-prey model. DNN prediction and direct integration results for x_1 from the initial value $x_1 = 3, x_2 = 2$. MC and MF represent Monte Carlo and manifold sampling methods, respectively.

Electronic dynamical process. A complex electronic circuit consists of many electronic components, such as resistors and capacitors. Numerical simulation of such a system describes the dynamical process of current and voltage. The ring modulator model of electronic circuits used in this example contains 15 composition elements with high nonlinearity and multiscale, and the integration step of a traditional solver is about 10^{-8}s . This model's detailed description and equations can be found in [36].

We first randomly sample 80,000 data points within the range, which is determined by the maximum and minimum value of each element contained by the traditional solver. Take these points as the initial conditions to evolve this system and sample 30 points randomly in the trajectory of 0.001s. The DNN we used consists of three hidden layers with sizes 800, 400, and 200, respectively. It maps the input vector contained in the current state and time to the state after $\Delta t = 10^{-6}\text{s}$.

For comparison, we randomly sample 2,400,000 data points within the same range to train another DNN with the same structure. The simulation results are shown in Fig. 3. It demonstrates that DeePODE

*<https://cantera.org/>

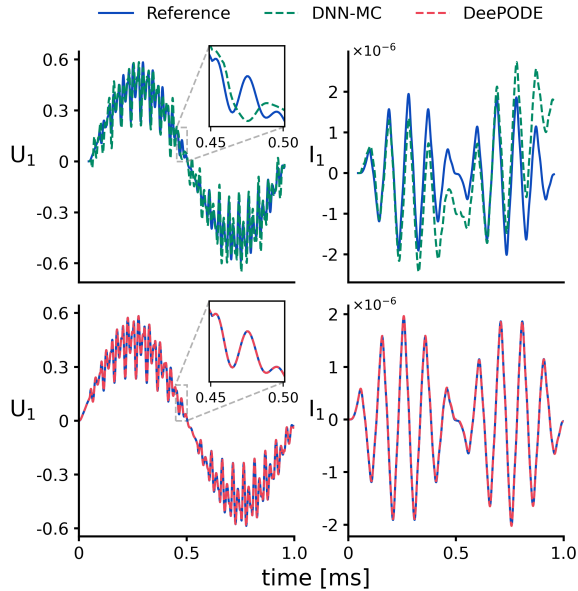


Fig. 3. Ring modulator model. DNN prediction and direct integration results for U_1 and I_2 .

can effectively solve this high-dimensional multiscale system while MC cannot deal with them well.

Battery electrolyte auto-ignition. Organic solvents, such as dimethyl carbonate (DMC), are the main components of lithium battery electrolytes. When overheated, the electrolytes decompose and release flammable gases. In this section, we apply DeePODE to sample from a DMC reaction mechanism with 102 species and 805 reactions, which is also used for simulating the laminar flame of gases vented from thermal runaway Li-ion batteries [37]. We then train a DNN surrogate model to accurately reproduce the DMC auto-ignition process under constant pressure.

We utilize Cantera to obtain the reference solution and generate datasets for DNN models. More specifically, for the MC method, 500,000 data points are sampled uniformly within the range temperature $\in [300, 3000]$, pressure $\in [0.5, 3]$ atm, species mass fraction $\in [0, 1]$. For the DeePODE method, we randomly pick 100,000 data points within the range above, and then for each sample, the state vector after Δt_i will be included in the input dataset, where $\Delta t_i \in \{10^{-6}, 10^{-5}, 10^{-4}, 10^{-3}\}$ s. The corresponding label datasets are obtained by evolving the input vectors for 10^{-6} s. We use the two datasets to train the corresponding neural networks with 1600,800,400 hidden neurons for three hidden layers, respectively. With the constraint of stiffness, the integration time step inside Cantera is 10^{-8} , while the DNN models predict the state after $\Delta t = 10^{-6}$ given an input state. Fig. 4 shows that samples by the DeePODE method can result in an accurate DNN model while the MC method does not.

Combustion examples. The simulation of multiscale combustion consists of two parts: fluid dynamics described by partial differential equations and chemical reactions described by high-dimensional stiff ODEs. The time scales of chemical reactions can vary across many orders of magnitudes [26], which makes the numerical simulation of chemical reactions extremely slow with a small time step. In the following, we apply the DeePODE method to obtain samples for training DNN surrogate models for the high-dimensional stiff ODEs

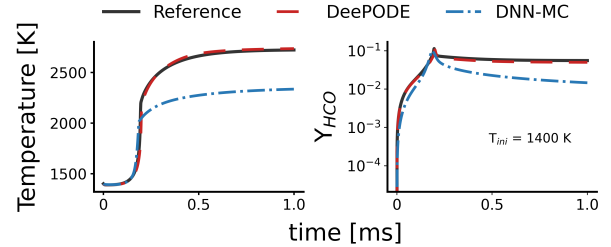


Fig. 4. Battery electrolyte auto-ignition of temperature and radical HCO mass fraction. The initial condition is $p_0 = 1$ atm, $T_0 = 1400$ K, equivalence ratio = 1.

in the simulation of combustion. The DeePODE models provide the change rate of chemical species as source terms for the simulation of CFD. The CFD code used in this part is EBI [38]. Detail information and examples with ASURF code [39, 40] or DeepFlame code [41] can be found in Appendix.

We test DeePODE models with various chemical mechanisms, such as GRI-Mech 3.0 with 53 species and 325 reactions for methane/air combustion, DRM19 with 21 species and 84 reactions for methane/air combustion, and an n-heptane mechanism consisting of 34 species and 191 reactions reduced by DeePMR [42] from a detailed mechanism with 116 species.

In this work, for each chemical mechanism, we train a DeePODE model[†] for all corresponding combustion examples.

In this section, we first show an example of data distribution obtained by different sampling methods. Then, we use a series of benchmark examples to demonstrate that our DeePODE models have good generalization. More examples, including zero-dimensional, one-dimensional, freely propagating premixed flame, two-dimensional counterflow, and triple flame, are shown in Appendix. Note that we do not show examples with Monte-Carlo sampling because they are completely unstable in combustion examples, which can be found in [8].

Data distribution for combustion. To justify the advantage of the DeePODE method, we visualize the datasets of DRM19 in the first two principal directions of the manifold dataset. As shown in Fig. 1(C), the distribution of the MC samples is homogeneous in different directions. With the DeePODE method evolving the governing equations, the obtained dataset, as shown on the right, has more samples of low change rate and fully covers the region of the manifold dataset (grey region). For the region with a low change rate, the reaction will stay in a small state range for a relatively long time. Therefore, the prediction accuracy in this low change rate region is very important. However, as a uniformly random method, MC can barely obtain samples in such a small region. This explains why neural networks trained by MC samples blow up at prediction (see examples in [8]) and DeePODE can accurately predict the combustion process.

Spherical flame example. The computational domain of the spherical flame, with size of $1\text{cm} \times 1\text{cm}$ and cells of 120,000, is filled with premixed gases characterized by a pressure of 1 atm and an equivalence ratio of 1. Different initial temperatures are imposed, while the ignition source is located at the center of the inlet with a radius of 0.4mm. As shown in Fig. 5(A), DeePODE models can capture the flame structure and propagation for GRI and n-heptane.

Turbulent ignition example. In the turbulent ignition case, we set 512×512 cells for the computational domain of $1.5\text{cm} \times 1.5\text{cm}$, the velocity field is generated by Passot-Pouquet isotropic kinetic energy

[†] DNN models are available at <https://github.com/intelligent-algorithm-team/intelligent-combustion>.

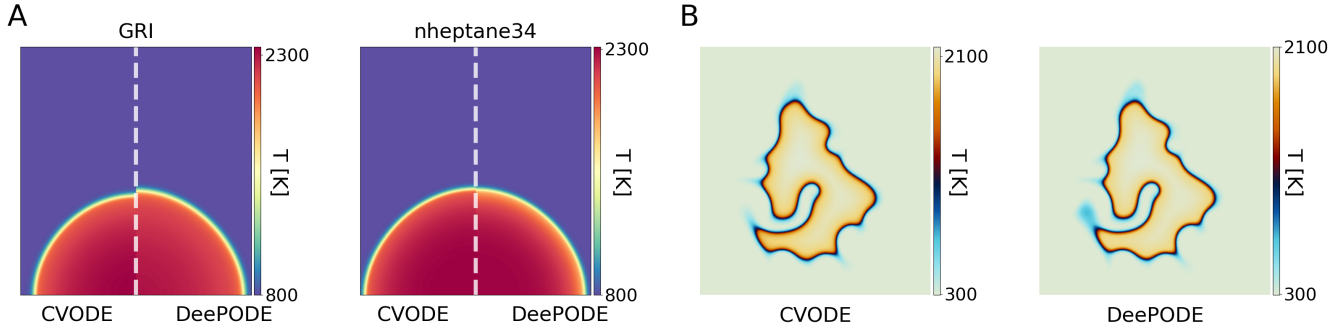


Fig. 5. Spherical flame and Turbulent ignition. (A) shows the temperature distribution of spherical flame by EBI with CVODE and DeePODE. The time point for GRI, n-heptane is 0.95ms, 1ms, respectively. (B) shows the temperature distribution by EBI with CVODE and DeePODE at 1.5ms for DRM19.

spectrum. We set an initial field with $T = 300\text{K}$, $P = 1\text{atm}$, $\phi = 1$ in the domain. The ignition round is set in the center of the domain with a radius of 0.4mm. As shown in Fig. 5(B), for DRM19, we show the temperature distribution by CVODE and Cantera at 1.5ms. The DeePODE model can capture the evolution of turbulent flame accurately.

Sandia flame D. Sandia flames are widely studied in many works [43, 1]. The Sandia flame D, which features a main jet comprising of CH_4 and air with an equivalence ratio of $\phi = 3.17$, bulk speed of $u_b = 49.6\text{m/s}$ via a nozzle with a diameter of 7.2mm, and the temperature $T = 294\text{K}$. The flame is stabilized with a pilot jet of C_2H_2 , H_2 , air, CO_2 , and N_2 , with a flow velocity of 11.4m/s. The pilot nozzle has inner and outer diameters of 7.7mm and 18.2mm, respectively. The jet inlets are surrounded by an air co-flow with an inner diameter of 18.9mm. The total number of cells is 2,000,000, and the chemical kinetic mechanism is DRM19. The details of the setup can be found in DLBFOam [44, 45]. In this example, we study the flame after ignition. Therefore, DeePODE is used after a certain time, i.e., 50ms in this example. For the area where the flame has not reached, the CVODE can use large step sizes, therefore, we do not apply DNN for those grids. The DeePODE is used for 100 thousand grids. As shown in Fig. 6(A), the case with DeePODE is not only stable but also very similar to the one with CVODE at different time snapshots. Quantitative comparison among DeePODE, CVODE, and experiment is shown in Fig. 6(B), which shows the average distributions of temperature, O_2 , CO_2 and velocity along the radial direction on one-dimensional cross-sections with axial value $x/d = 1, 30, 60$.

Time cost. We compare the cost time of computing reaction rates in one step in each example using a single CPU (Intel(R) Xeon(R) Platinum 8260 CPU@2.40GHz) or single GPU (Tesla V100-SXM2-32GB). As shown in Table 1 in the Appendix, GPU can accelerate the computation of reaction rates by more than one order of magnitude for all cases. Compared with DRM19, GRI and n-heptane have more species, and the acceleration is much more significant, i.e., more than two orders of magnitude. The key reason for the acceleration is that the DeePODE model uses matrix computation, which is excellent for parallel computation when the matrix size is large.

Discussion. This work proposes a DeePODE method for solving high-dimensional multiscale dynamical systems by machine learning. We demonstrate the effectiveness of the DeePODE method by training DNN surrogate models for various systems. For example,

DNN models are trained in combustion simulation with only data from zero- and one-dimensional experiments. However, they can generalize well to two- and three-dimensional combustion simulations with various conditions, even to turbulent combustion. This surprising generalization ability arises from the multiscale property embedded in the samples by the DeePODE method. Extensive simulations in this work show the great potential of the DeePODE method in fast and accurately solving high-dimensional multiscale dynamical systems.

ACKNOWLEDGMENTS. This work is sponsored by the National Key R&D Program of China Grant No. 2022YFA1008200 (Z. X., Y. Z.), the National Natural Science Foundation of China Grant No. 12101402 (Y. Z.), No. 62002221 (Z. X.), the Lingang Laboratory Grant No. LG-QS-202202-08 (Y. Z.), Shanghai Municipal of Science and Technology Project Grant No. 20JC1419500 (Y. Z.), Shanghai Municipal of Science and Technology Major Project No. 2021SHZDZX0102, and the HPC of School of Mathematical Sciences and the Student Innovation Center, the Siyuan-1 cluster supported by the Center for High-Performance Computing at Shanghai Jiao Tong University.

References

- Barlow R, Frank J (1998) Effects of turbulence on species mass fractions in methane/air jet flames in *Symposium (International) on Combustion*. (Elsevier), Vol. 27, pp. 1087–1095.
- McAdams HH, Shapiro L (1995) Circuit simulation of genetic networks. *Science* 269(5224):650–656.
- Volterra V (1931) Variations and fluctuations of the number of individuals in animal species living together. *Animal ecology* pp. 412–433.
- Ye H, Liu Y, Zhang P, Du Z (2016) Analysis and detection of forced oscillation in power system. *IEEE Transactions on Power Systems* 32(2):1149–1160.
- Sun Y, Zhou D, Rangan AV, Cai D (2009) Library-based numerical reduction of the hodgkin–huxley neuron for network simulation. *Journal of computational neuroscience* 27:369–390.
- Dissanayake M, Phan-Thien N (1994) Neural-network-based approximations for solving partial differential equations. *communications in Numerical Methods in Engineering* 10(3):195–201.
- Raissi M, Perdikaris P, Karniadakis GE (2019) Physics-informed neural networks: A deep learning framework for solving forward and inverse problems involving nonlinear partial differential equations. *Journal of Computational Physics* 378:686–707.
- Zhang T, et al. (2022) A multi-scale sampling method for accurate and robust deep neural network to predict combustion chemical kinetics. *Combustion and Flame* 245:112319.
- Li S, McLaughlin DW, Zhou D (2023) Mathematical modeling and analysis of spatial neuron dynamics: Dendritic integration and beyond. *Communications on Pure and Applied Mathematics* 76(1):114–162.

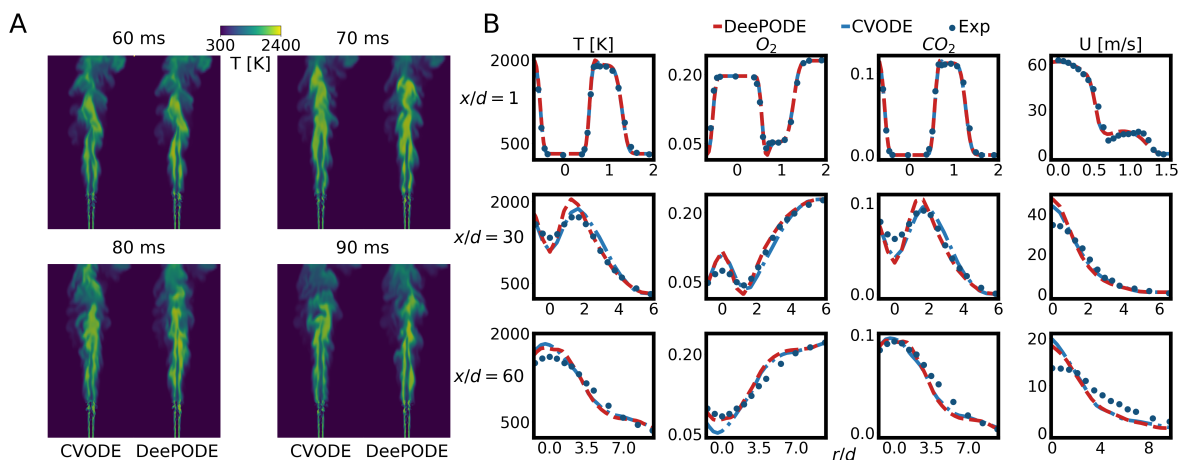


Fig. 6. Sandia flame D example. (A) shows the snapshots of temperature distribution by EBI with CVODE or DeePODE for DRM19 at different time. (B) compares the average distributions of temperature, O_2 , CO_2 and velocity by DeePODE, CVODE and experiment along radial direction on different axial locations .

10. Milman VD, Schechtman G (2009) *Asymptotic theory of finite dimensional normed spaces: Isoperimetric inequalities in riemannian manifolds.* (Springer) Vol. 1200.
11. Chen JY, Kollmann W, Dibble R (1989) Pdf modeling of turbulent non-premixed methane jet flames. *Combustion Science and Technology* 64(4-6):315–346.
12. Pope SB (1997) Computationally efficient implementation of combustion chemistry using in situ adaptive tabulation.
13. Christo F, Masri A, Nebot E (1996) Artificial neural network implementation of chemistry with pdf simulation of h2/co2 flames. *Combustion and Flame* 106(4):406–427.
14. Blasco J, Fueyo N, Dopazo C, Ballester J (1998) Modelling the temporal evolution of a reduced combustion chemical system with an artificial neural network. *Combustion and Flame* 113(1-2):38–52.
15. Choi Y, Chen JY (2005) Fast prediction of start-of-combustion in hcci with combined artificial neural networks and ignition delay model. *Proceedings of the Combustion Institute* 30(2):2711–2718.
16. Sen BA, Menon S (2010) Linear eddy mixing based tabulation and artificial neural networks for large eddy simulations of turbulent flames. *Combustion and Flame* 157(1):62–74.
17. Sinaei P, Tabejamaat S (2017) Large eddy simulation of methane diffusion jet flame with representation of chemical kinetics using artificial neural network. *Proceedings of the Institution of Mechanical Engineers, Part E: Journal of Process Mechanical Engineering* 231(2):147–163.
18. Zhang T, Zhang Y, E W, Ju Y (2021) A deep learning-based ode solver for chemical kinetics in *AIAA Science and Technology Forum and Exposition, AIAA SciTech Forum 2021.* (American Institute of Aeronautics and Astronautics Inc, AIAA).
19. Owoyeye O, Pal P (2022) Chemnode: A neural ordinary differential equations framework for efficient chemical kinetic solvers. *Energy and AI* 7:100118.
20. Almeldein A, Van Dam N (2022) Accelerating chemical kinetics calculations with physics informed neural networks in *Internal Combustion Engine Division Fall Technical Conference.* (American Society of Mechanical Engineers), Vol. 86540, p. V001T06A007.
21. De Florio M, Schiassi E, Furfaro R (2022) Physics-informed neural networks and functional interpolation for stiff chemical kinetics. *Chaos: An Interdisciplinary Journal of Nonlinear Science* 32(6):063107.
22. Yao S, Kronenburg A, Shamooni A, Stein O, Zhang W (2022) Gradient boosted decision trees for combustion chemistry integration. *Applications in Energy and Combustion Science* 11:100077.
23. Silver D, et al. (2016) Mastering the game of go with deep neural networks and tree search. *nature* 529(7587):484–489.
24. Noé F, Olsson S, Köhler J, Wu H (2019) Boltzmann generators: Sampling equilibrium states of many-body systems with deep learning. *Science* 365(6457):eaaw1147.
25. Hawkes ER, Sankaran R, Sutherland JC, Chen JH (2005) Direct numerical simulation of turbulent combustion: fundamental insights towards predictive models in *Journal of Physics: Conference Series.* (IOP Publishing), Vol. 16, p. 65.
26. Lu T, Law CK (2009) Toward accommodating realistic fuel chemistry in large-scale computations. *Progress in Energy and Combustion Science* 35(2):192–215.
27. Chi C, Janiga G, Thévenin D (2021) On-the-fly artificial neural network for chemical kinetics in direct numerical simulations of premixed combustion. *Combustion and Flame* 226:467–477.
28. Ding T, Readshaw T, Rigopoulos S, Jones W (2021) Machine learning tabulation of thermochemistry in turbulent combustion: An approach based on hybrid flamelet/random data and multiple multilayer perceptrons. *Combustion and Flame* 231:111493.
29. Mettler MS, Vlachos DG, Dauenhauer PJ (2012) Top ten fundamental challenges of biomass pyrolysis for biofuels. *Energy & Environmental Science* 5(7):7797–7809.
30. Seinfeld JH, Pandis SN (1998) From air pollution to climate change. *Atmospheric chemistry and physics* 1326.
31. Maas U, Pope SB (1992) Simplifying chemical kinetics: intrinsic low-dimensional manifolds in composition space. *Combustion and flame* 88(3-4):239–264.
32. Box GE, Cox DR (1964) An analysis of transformations. *Journal of the Royal Statistical Society: Series B (Methodological)* 26(2):211–243.
33. Xu ZQJ, Zhang Y, Xiao Y (2019) Training behavior of deep neural network in frequency domain. *International Conference on Neural Information Processing* pp. 264–274.
34. Xu ZQJ, Zhang Y, Luo T, Xiao Y, Ma Z (2020) Frequency principle: Fourier analysis sheds light on deep neural networks. *Communications in Computational Physics* 28(5):1746–1767.
35. Qin T, Chen Z, Jakeman JD, Xiu D (2021) Data-driven learning of nonautonomous systems. *SIAM Journal on Scientific Computing* 43(3):A1607–A1624.
36. Timofeev KA, Shornikov YV (2022) Computer simulation of dynamic processes in electronic systems in *2022 IEEE International Multi-Conference on Engineering, Computer and Information Sciences (SIBIRCON).* pp. 1860–1863.
37. Johnsplass J, Henriksen M, Vaagsaether K, Lundberg J, Bjerketvedt D (2017) Simulation of burning velocities in gases vented from thermal run-a-way lithium ion batteries in *Linköping Electronic Conference Proceedings, Proceedings of the 58th Conference on Simulation and Modelling (SIMS 58) Reykjavik, Iceland, September 25th – 27th, 2017.*
38. Zirwes T, et al. (2020) Quasi-dns dataset of a piloted flame with inhomogeneous inlet conditions. *Flow, Turbulence and Combustion* 104(4):997–1027.

39. Chen Z, Burke MP, Ju Y (2009) Effects of lewis number and ignition energy on the determination of laminar flame speed using propagating spherical flames. *Proceedings of the Combustion Institute* 32(1):1253–1260.
40. Zhang T, Susa AJ, Hanson RK, Ju Y (2021) Studies of the dynamics of autoignition assisted outwardly propagating spherical cool and double flames under shock-tube conditions. *Proceedings of the Combustion Institute* 38(2):2275–2283.
41. Mao R, et al. (2022) Deepflame: A deep learning empowered open-source platform for reacting flow simulations. *arXiv preprint arXiv:2210.07094*.
42. Wang Z, et al. (2022) A deep learning-based model reduction (deepmr) method for simplifying chemical kinetics.
43. Schneider C, Dreizler A, Janicka J, Hassel E (2003) Flow field measurements of stable and locally extinguishing hydrocarbon-fuelled jet flames. *Combustion and Flame* 135(1-2):185–190.
44. Morev I, et al. (2022) Fast reactive flow simulations using analytical jacobian and dynamic load balancing in OpenFOAM. *Physics of Fluids* 34(2):021801.
45. Tekgül B, Peltonen P, Kahila H, Kaario O, Vuorinen V (2021) Dlbfoam: An open-source dynamic load balancing model for fast reacting flow simulations in openfoam. *Computer Physics Communications* p. 108073.